

Drifting plasmons in open two-dimensional channels: modal analysis

O Sydoruk

Optical and Semiconductor Devices Group, Department of Electrical and Electronic Engineering, Imperial College London, South Kensington Campus, London SW7 2AZ, UK

E-mail: osydoruk@imperial.ac.uk

Received 28 November 2012, in final form 1 February 2013

Published 28 February 2013

Online at stacks.iop.org/JPhysD/46/135103

Abstract

Understanding the properties of plasmons in two-dimensional channels is important for developing methods of terahertz generation. This paper presents a modal analysis of plasmonic reflection in open channels supporting dc currents. As it shows, the plasmons can be amplified upon reflection if a dc current flows away from a conducting boundary; de-amplification occurs for the opposite current direction. The problem is solved analytically, based on a perturbation calculation, and numerically, and agreement between the methods is demonstrated. The power radiated by a channel is found to be negligible, and plasmon reflection in open channels is shown to be similar to that in closed channels. Based on this similarity, the oscillator designs developed earlier for closed channels could be applicable also for open ones. The results develop the modal-decomposition technique further as an instrument for the design of terahertz plasmonic sources.

(Some figures may appear in colour only in the online journal)

1. Introduction

The potential of semiconductor plasmas for sources of electromagnetic radiation has been attracting attention for over half a century. Early work in the 1960s concentrated on the analogy between electrons in solids and in vacuum electron beams. The effects considered include the two-stream instability [1] and travelling-wave interactions with acoustic [2] and optical [3] phonons and with artificial slow-wave structures [4]. Experiments on the low-frequency acoustic-wave amplifier [2] demonstrated the feasibility of the approach but were eventually eclipsed by the progress in transistors and diodes. Advances in fabrication revived the activity in the late 1970s and in 1980s [5–7]. On the other hand, the most recent upsurge of the interest in semiconductor plasmas [8–10] has been motivated by the progress in the terahertz (THz) technology and the need for new THz sources. Generation mechanisms, such as travelling-wave interactions with slow-wave structures [11, 12] and optical phonons [13–16], have been revisited. Considerable attention has also been paid to the plasma instability in field-effect transistors, whose original treatment by Dyakonov and Shur [17] was further developed by considering electron diffusion [18], non-uniform channels [19, 20] and alternative geometries [18, 21, 22].

The behaviour of field-effect transistors, like that of transit-time devices [23, 24], is determined by the channel boundaries. The boundary conditions postulated by Dyakonov and Shur [17] and adopted by the majority of studies are zero ac potential at the source and zero ac current at the drain. Although attractively simple, this approach is limited in several ways. First, it defines the boundary conditions only at the channel, ignoring the transverse distribution of the plasmonic fields. Second and more important, it provides no recipe of how these postulated conditions could be achieved. A more advanced theoretical model is, therefore, desirable to describe the plasmon behaviour at realistic boundaries and help design plasmonic oscillators.

A promising alternative approach, introduced recently [25, 26], is based on mode decomposition. It can be summarized as follows. A plasmon incident in a two-dimensional channel on a boundary (say, a perfect conductor) will scatter, in the presence of a dc current, not only into a single reflected plasmon but also into all eigenmodes propagating in the opposite direction. The fields at the boundary are given by the superposition of the incident and all reflected modes. The modal reflection coefficients are then determined from the rigorous electrodynamic boundary condition of no tangential electric field. The model can also be generalized for

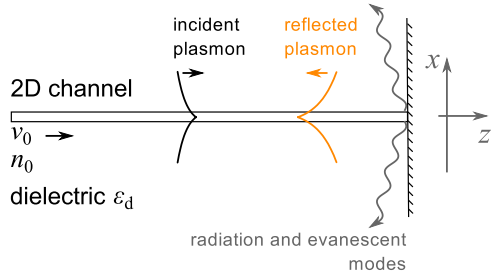


Figure 1. When a dc current flows through a two-dimensional channel, the plasmons propagating along and against the current have different field distributions. As a result, a plasmon incident on a conducting boundary excites not only a single reflected plasmon but a spectrum of eigenmodes, including radiation and evanescent modes.

junctions between two different channels [25], where the fields at the boundaries are given by the superposition of an incident, reflected, and transmitted modes, whose modal coefficients are found from (again, electrostatically rigorous) conditions of field continuity at the junction plane. The knowledge of the reflection and transmission coefficients can be further used to design plasmonic oscillators, for example, comprising distributed reflectors [25] or conducting boundaries combined with two different channels [26].

Whereas [25, 26] have established the foundation of the mode-decomposition technique for drifting plasmons, they considered only closed structures. Most practical configurations are, however, open and have to be studied separately [27, 28].

As a step towards practical configurations, this paper describes the reflection of plasmons propagating in open two-dimensional channels, figure 1. The discussion will follow the steps of the standard decomposition technique [27, 28], which has, however, to be revisited to include the effects of dc currents. Section 2 considers the mode spectrum in a two-dimensional channel. It discusses the properties of drifting plasmons and of radiation and evanescent modes. Section 3 considers reflection of a plasmon from a conducting boundary. It formulates and solves the mode-decomposition problem, deriving the values of the plasmonic reflection coefficients and demonstrating plasmonic amplification. Section 4 draws conclusions.

2. Mode spectrum in channels with dc current

This section discusses an infinitely long channel with a dc current and the its eigenmode spectrum. The channel with the dc electron density of n_0 occupies the plane $x = 0$. Electrons in the channel can drift with the dc velocity v_0 , whose sign determines the direction. The dc current density is $J_0 = en_0v_0$, where e is the electron charge. A dielectric with the relative permittivity ϵ_d surrounds the channel.

Drifting electrons can interact with electromagnetic waves that have a longitudinal component of the electric field, and so TM waves will be assumed, with the electric field components E_x and E_z and the magnetic field component H_y . Above and below the channel, the waves obey Maxwell's equations

yielding the dispersion relation

$$k_z^2 + k_x^2 = k_0^2 \epsilon_d, \quad (1)$$

where k_z and k_x are the longitudinal and the transverse wavenumbers, respectively, and $k_0 = \omega/c$, with the angular frequency $\omega = 2\pi f$ and the vacuum light velocity c . At the channel, the fields obey the standard electrodynamic boundary conditions for the normal component of the displacement

$$E_x|_{x=+0} - E_x|_{x=-0} = \frac{en}{\epsilon_0 \epsilon_d}, \quad (2)$$

and the tangential component of the magnetic field

$$H_y|_{x=+0} - H_y|_{x=-0} = J. \quad (3)$$

Here, n and J are, respectively, the ac electron and current densities. The standard expression for the linearized current density is [12, 16, 17, 22]

$$J = en_0v + env_0, \quad (4)$$

where v is the ac electron velocity for which the linearized equation of motion yields

$$v = -j \frac{e}{m} \frac{E_z|_{x=0}}{\omega - k_z v_0}, \quad (5)$$

where j is the imaginary unit, and m is the effective electron mass. The time variation is in the form $\exp(j\omega t)$ and the spatial variation is in the form $\exp(-jk_x x - jk_z z)$.

Equation (5) ignores collisions and diffusion, which limits its validity to low temperatures. This approach is, nevertheless, desirable for the present analysis. Central to the discussion below will be the question of power carried by individual modes as well as that of power exchange between the modes. The total power of a mode is the sum of its electromagnetic and kinetic powers, which could flow in opposite directions. The issue is complicated enough without considering power dissipation. In addition, collisions can give rise to the resistive-wall instability [29], which would further obscure the effects considered here.

Another limitation of (5) is low drift velocities. As experiments at drift velocities approaching the saturation value showed [30], plasmons can deviate from the behaviour given by the term $\omega - k_z v_0$. However, the effects considered here appear at low drift velocities; the maximum value of v_0 used in the calculations below was $6 \times 10^6 \text{ cm s}^{-1}$, five times less than the maximum drift velocity in GaAs.

The next step is to find the eigenmodes subject to the condition that their amplitudes remain finite at $x = \pm\infty$. It will be done, following the standard approach [27, 28], by assuming a frequency ω and finding the permissible values of the wavenumbers k_x and k_z . Due to the transverse symmetry, see figure 1, the modes can be separated into even and odd ones.

2.1. Odd modes

The fields of the odd modes are of the form

$$\begin{aligned} E_x &= \pm (Ae^{-jk_x x} + Be^{jk_x x}) e^{-jk_z z} \\ H_y &= \pm \frac{\omega \epsilon_0 \epsilon_d}{k_z} (Ae^{-jk_x x} + Be^{jk_x x}) e^{-jk_z z} \\ E_z &= \pm \frac{k_x}{k_z} (-Ae^{-jk_x x} + Be^{jk_x x}) e^{-jk_z z}, \end{aligned} \quad (6)$$

where the plus sign corresponds to the fields above the channel and the minus sign, to the fields below it. Here and in the following, the harmonic time variation is, as usual, implied. Substituting the above equations into the boundary conditions (2) and (3) yields

$$\begin{aligned} E_x &= \pm A [(1 - \Gamma)e^{-jk_x x} - (1 + \Gamma)e^{jk_x x}] e^{-jk_z z} \\ &= \mp 2A [\Gamma \cos(k_x x) + j \sin(k_x x)] e^{-jk_z z} \end{aligned} \quad (7)$$

where

$$\Gamma = -j \frac{e^2 n_0}{2m \epsilon_0 \epsilon_d} \frac{k_x}{(\omega - k_z v_0)^2}. \quad (8)$$

In principle, the transverse wavenumber could be complex, so that $k_x = k'_x + jk''_x$. As analysis shows, however, the condition that the fields remain finite restricts the permissible range of k_x to either purely real or purely imaginary values. It separates the spectrum into two parts, a discrete and a continuous ones, as discussed next.

2.1.1. Discrete spectrum: plasmons. Purely imaginary transverse wavenumbers ($k_x = -j\kappa_x$, where κ_x is real and positive) correspond to plasmons. The amplitudes of the relevant ac quantities for $x \geq 0$ take then the form

$$\begin{aligned} E_x &= Ae^{-\kappa_x x - jk_z z} \\ H_y &= A \frac{\omega \epsilon_0 \epsilon_d}{k_z} e^{-\kappa_x x - jk_z z} \\ v &= A \frac{e}{m} \frac{\kappa_x}{k_z (\omega - k_z v_0)} e^{-jk_z z} \\ J &= 2A \frac{\omega \epsilon_0 \epsilon_d}{k_z} e^{-jk_z z}. \end{aligned} \quad (9)$$

The plasmons obey, from (7), the condition $1 + \Gamma = 0$ or

$$(\omega - k_z v_0)^2 = \Omega_p^2 \kappa_x, \quad (10)$$

where $\Omega_p = e^2 n_0 / (2m \epsilon_0 \epsilon_d)$. Equation (10) is the classical dispersion relation for two-dimensional plasmons [31] when $v_0 = 0$. The implications of drift were more recently discussed by Crowne [18]. The values of k_z and κ_x are not independent of each other but linked by (1), the dispersion relation in the dielectric. In particular, the condition $\kappa_x = 0$, which would set the right-hand side of (10) to zero, implies, from (1), $k_z = \sqrt{\epsilon_d} \omega / c$ leading to the left-hand side in the form $\omega(1 - \sqrt{\epsilon_d} v_0 / c)$. Because $v_0 \ll c$, the left-hand side of (10) does not vanish, $\omega - k_z v_0 \neq 0$. As a result, no singularities will occur in (9).

Given (1), the dispersion relation (10) has, at any frequency, four solutions for k_z , each representing a plasmon.

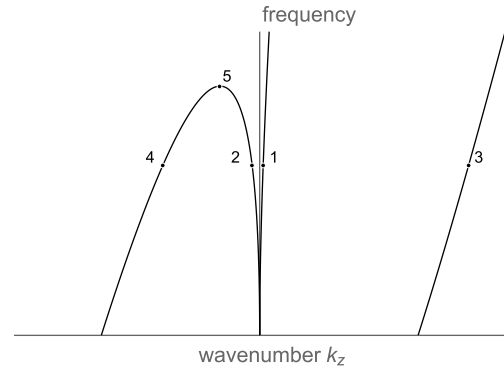


Figure 2. In the presence of dc current, four plasmons can propagate along the channel. All four have real wavenumbers below point 5. The plasmons denoted by points 1–4 have different wavenumbers. Plasmons 1, 3 and 4 propagate along the drift; plasmon 2 propagates against the drift.

Their typical dispersion curves are shown in figure 2 for positive v_0 and for real k_z . Most notably, the dispersion curves are different for positive and negative values of k_z . Due to the linkage between k_z and κ_x , the transverse field distributions of plasmons propagating in opposite directions are also different, see figure 1. As a result—and in stark contrast to the driftless channel—a plasmon incident on a perfectly conducting boundary cannot scatter into a single reflected plasmon. Nor, as will be shown below, do the incident and the reflected plasmons have equal amplitudes.

Because this paper concentrates on relatively low drift velocities, it will discuss plasmon reflection for frequencies below the one that corresponds to point 5 on the dispersion diagram, figure 2. When the drift velocity decreases, point 5 moves to the left and upwards, thus increasing the frequency range covered by the analysis. In this range, four plasmons propagate with real values of k_z . As their group velocities suggest, the plasmons corresponding to points 1, 3, and 4 propagate in the positive z -direction (along the electron drift), whereas the plasmon corresponding to point 2 propagates in the negative z -direction. Hence, when plasmon 1 is incident on a conducting boundary, it will excite a single reflected plasmon 2. However, when plasmon 2 is incident, it will excite three reflected plasmons, plasmon 1, plasmon 3 and plasmon 4.

Further observations about the plasmon reflection can be made by examining the dispersion diagram. Plasmons 1 and 2 have comparable absolute values of the wavenumbers, and, hence, similar field distributions. Their wavenumbers, however, differ from those of plasmons 3 and 4. For example, $k_{z1} = 16 \text{ rad } \mu\text{m}^{-1}$, $k_{z2} = -35 \text{ rad } \mu\text{m}^{-1}$, $k_{z3} = 978 \text{ rad } \mu\text{m}^{-1}$, $k_{z4} = -457 \text{ rad } \mu\text{m}^{-1}$ for the channel with $n_0 = 10^{11} \text{ cm}^{-2}$, $v_0 = 5 \times 10^6 \text{ cm s}^{-1}$, $\epsilon_d = 12.8$, $m = 0.067m_0$ (corresponding to GaAs), and $f = 1 \text{ THz}$. As a result, only plasmons 1 and 2 can scatter effectively into each other and provide a sustained reflection pattern in resonators. This paper will, therefore, concentrate on the interplay between these two plasmons, although all four will be included in the numerical calculations.

2.1.2. Continuous spectrum: radiation and evanescent modes. When k_x is purely real, the relevant ac quantities take the form

for $x \geq 0$

$$\begin{aligned} E_x &= -2A[\Gamma \cos(k_x x) + j \sin(k_x x)]e^{-jk_z z} \\ H_y &= -2A \frac{\omega \varepsilon_0 \varepsilon_d}{k_z} [\Gamma \cos(k_x x) + j \sin(k_x x)]e^{-jk_z z} \\ v &= 2jA \frac{e}{m} \frac{k_x}{k_z (\omega - k_z v_0)^2} e^{-jk_z z} \\ J &= 4jA \frac{\omega \varepsilon_0 \varepsilon_d}{k_z} \Gamma e^{-jk_z z}. \end{aligned} \quad (11)$$

Unlike the discrete set of four values for the plasmons, k_x can now have arbitrary real values ranging from 0 to ∞ . These modes build a continuous part of the spectrum. From (1), both k_x and k_z are real for $0 < k_x < \sqrt{\varepsilon_d} k_0$. The corresponding values of k_z are $0 < k_z < \sqrt{\varepsilon_d} k_0$. These radiation modes can propagate along the z - and x -directions and are not bound to the channel. Analogously to the plasmons, for the radiation modes one obtains $\omega - k_z v_0 \geq \omega(1 - \sqrt{\varepsilon_d} v_0/c) \neq 0$ due to the small values of the electron drift velocity v_0 . As a result, no singularities occur in (11). For $k_x > \sqrt{\varepsilon_d} k_0$, k_z is imaginary corresponding to evanescent modes that decay along the channel.

2.2. Even modes

For even modes, the transverse electric field component is in the form

$$E_x = (A e^{-jk_x x} + B e^{jk_x x}) e^{-jk_z z} \quad (12)$$

both above and below the channel; the other ac components can be derived following the same steps as for the odd modes. Applying the boundary conditions (2) and (3) and the condition that the fields are finite at $x = \pm\infty$, one obtains

$$\begin{aligned} E_x &= A \cos(k_x x) e^{-jk_z z} \\ H_y &= A \frac{\omega \varepsilon_0 \varepsilon_d}{k_z} \cos(k_x x) e^{-jk_z z} \\ v &= 0 \\ J &= 0. \end{aligned} \quad (13)$$

Similar to the odd modes, the even modes build a continuous spectrum with arbitrary real k_x . The even modes, however, do not couple to the drifting electrons. In addition, the plasmons, being odd modes, can scatter only in other odd modes. The even modes can, therefore, be ignored in the following discussion.

2.3. Mode power

The total ac power carried by a mode can be written as the following sum [26, 32, 33]:

$$P = \text{Re} \int_0^\infty E_x H_y^* dx + \frac{m v_0}{2e} \text{Re}(v J^*), \quad (14)$$

where the asterisk denotes complex conjugation. The first term in (14) is the electromagnetic power due to the fields, and the second term, proportional to the drift velocity v_0 , is the kinetic power due to the electron movement. Substituting the

expressions for the ac plasmonic quantities (9) into (14) yields the power carried by a plasmon in the form

$$P_{\text{plasmon}} = |A|^2 \frac{\omega \varepsilon_0 \varepsilon_d}{k_z \kappa_x} \left[\frac{1}{2} + \frac{v_0 \kappa_x^2}{k_z (\omega - k_z v_0)} \right]. \quad (15)$$

The total power of an odd mode from the continuous spectrum can be written invoking the delta function, as it is done for passive waveguides [28], in the form

$$P = 2\pi \omega \varepsilon_0 \varepsilon_d \frac{\text{Re} k_z}{k_z^2} (1 + |\Gamma|^2) |A|^2 \delta(k_z - \tilde{k}_z^*), \quad (16)$$

where k_z and \tilde{k}_z are two wavenumbers. The power of the radiation modes, with real k_z , is hence

$$P_{\text{radiation}} = 2\pi \frac{\omega \varepsilon_0 \varepsilon_d}{k_z} (1 + |\Gamma|^2) |A|^2 \delta(k_z - \tilde{k}_z^*). \quad (17)$$

On the other hand, the power of the evanescent modes, with imaginary k_z , is zero. Separately, however, the electromagnetic and the kinetic power of the evanescent modes are non-zero, but are equal and carried in opposite directions.

3. Reflection from a conducting boundary

As has already been discussed, the spectra of the waves propagating in the opposite directions are different. A single plasmon incident on a perfectly conducting boundary excites not a single reflected plasmon but all possible reflected waves. Assuming the dc current flowing towards the boundary placed at $z = 0$, the boundary condition of zero total electric field component E_x can be written in the form

$$e^{-\kappa^{(+)} x} + R e^{-\kappa^{(-)} x} - 2 \int_0^\infty r(k_x) [\Gamma \cos(k_x x) + j \sin(k_x x)] dk_x = 0 \quad (18)$$

The first term represents the incident plasmon with unit amplitude. The second term represents the reflected plasmon, where R is the reflection coefficient. The third term, the integral, represents the continuous spectrum of the reflected modes, where $r(k_x)$ is their reflection coefficient. When the dc current flows away from the boundary, the boundary condition will have the same form but with three reflected plasmons, see section 2.1.1.

The reflection coefficients are found below, first, analytically by a perturbation approach and, second, numerically.

3.1. Analytic solution

For small drift velocity v_0 , the solutions of (18) will differ little from the driftless solutions. Hence, expanding in the Taylor series and retaining only the terms proportional to the drift velocity, one can write

$$\begin{aligned} \kappa^{(+)} &= \kappa^{(0)} + \delta \kappa^{(+)} \cdot v_0 \\ \kappa^{(-)} &= \kappa^{(0)} + \delta \kappa^{(-)} \cdot v_0 \\ R &= -1 + \delta R \cdot v_0 \\ r(k_x) &= 0 + \delta r(k_x) \cdot v_0 \\ \Gamma &= \Gamma^{(0)} + \delta \Gamma \cdot v_0, \end{aligned} \quad (19)$$

where the absolute values of the second terms on the right-hand sides are small, and the superscript (0) refers to the driftless values. Substituting (19) into the dispersion relation (10) and ignoring the terms proportional to v_0^2 yields

$$\delta\kappa^{(+)} = -\delta\kappa^{(-)} = -\frac{2\kappa^{(0)2}}{\omega}. \quad (20)$$

Substituting (19) into (18), expanding the exponentials in the Taylor series, and ignoring again the terms proportional to v_0^2 yields

$$\delta r(k_x) e^{-\kappa^{(0)}x} + (\delta\kappa^{(-)} - \delta\kappa^{(+)})x e^{-\kappa^{(0)}x} - 2 \int_0^\infty \delta r(k_x) [\Gamma^{(0)} \cos(k_x x) + j \sin(k_x x)] dx = 0 \quad (21)$$

Multiplying (21) by $e^{-\kappa^{(0)}x}$, integrating over x , using the orthogonality conditions for the driftless modes and (20) yields the plasmon reflection coefficient in the form

$$R = -1 - \frac{2\kappa^{(0)}v_0}{\omega}. \quad (22)$$

One the other hand, multiplying (21) by $\tilde{\Gamma}^{(0)} \cos(\tilde{k}_x x) + j \sin(\tilde{k}_x x)$ and doing the same as above yields for the reflection coefficient of the modes from the continuous spectrum

$$r(k_x) = -\frac{4j}{\pi} \frac{k_x v_0 \kappa^{(0)3}}{\omega [k_x^2 + \kappa^{(0)2}]^2}. \quad (23)$$

Equations (22) and (23) are the solutions also when the dc current flows away from the boundary.

3.2. Numerical solution

Similar to the standard approach of the mode-decomposition technique, a numerical solution of (18) can be obtained as follows. First, the spatial variation is eliminated by multiplying (18) by the eigenmode functions, (9) and (11), and integrating it over the x coordinate. Usually, the mode orthogonality simplifies the result, but for the channel with a dc current, a single boundary condition appears to be insufficient to employ the orthogonality relationship [26, 34]. Thus, multiplying (18) by $\exp(-\kappa^{(-)}x)$ and integrating over x yields

$$0 = \frac{1}{\kappa^{(+)} + \kappa^{(-)}} + \frac{R}{2\kappa^{(-)}} - 2j \int_0^\infty r(k_x) \frac{k_x v_0}{k_z + k_z^{(-)}} \frac{2\omega - [k_z + k_z^{(-)}] v_0}{(\omega - k_z v_0)^2} dk_x. \quad (24)$$

Multiplying (18) by $\Gamma_\beta \cos(k_{x\beta}x) + j \sin(k_{x\beta}x)$ yields

$$0 = j \frac{k_{x\beta} v_0}{k_{z\beta} + k_z^{(+)}} \frac{2\omega - [k_{z\beta} + k_z^{(+)}] v_0}{(\omega - k_{z\beta} v_0)^2} + jR \frac{k_{x\beta} v_0}{k_{z\beta} + k_z^{(-)}} \times \frac{2\omega - [k_{z\beta} + k_z^{(-)}] v_0}{(\omega - k_{z\beta} v_0)^2} + \pi \left[1 + \frac{\Omega_p^4 k_{z\beta}^2}{(\omega - k_{z\beta} v_0)^4} \right] r(k_{z\beta}) - 2\Omega_p^2 \frac{k_{x\beta} v_0}{(\omega - k_{z\beta} v_0)^2} \int_0^\infty r(k_x) \frac{k_x}{k_z + k_{z\beta}} \times \frac{2\omega - (k_z + k_{z\beta}) v_0}{(\omega - k_z v_0)^2} dk_x. \quad (25)$$

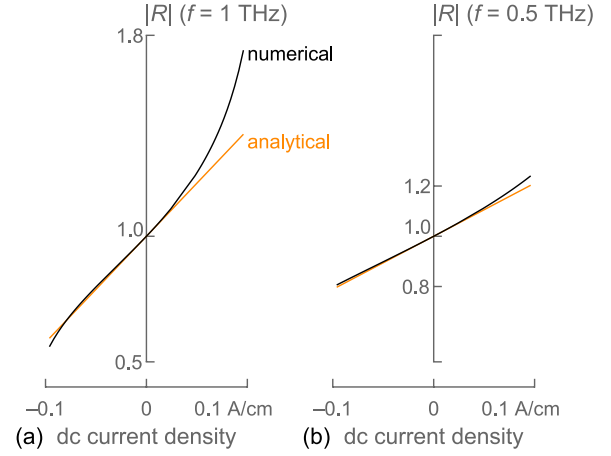


Figure 3. Plasmonic reflection coefficients depend on the magnitude and the direction of the dc current. The dependence is stronger for 1 THz (a) than for 0.5 THz (b).

The second step is to discretize the integrals in (24) and (25) and take a large value of k_x as the upper limit. The simplest discretization is in the form

$$\int_0^\infty f(k_x) dk_x \approx \Delta k_x \sum_{\alpha=1}^N f(k_{x\alpha}), \quad (26)$$

where $\Delta k_x = k_{x\alpha+1} - k_{x\alpha}$. As a result, (24) and (25) transform into an $(N+1) \times (N+1)$ matrix equation of the form $\mathbf{A} \cdot (R, r_1, r_2, \dots, r_N)^T = \mathbf{B}$. The formulation is analogous when the dc current flows away from the interface, but with three reflected plasmons.

3.3. Example: amplification of the reflected plasmons

The numerical and analytical solutions can be employed for various configurations. The parameters of the most interest are the frequency and the dc current density (drift velocity). For the frequency, the values 0.5 and 1 THz were chosen. The drift velocity varied from 0 to $v_0 = \pm 6 \times 10^6 \text{ cm s}^{-1}$, corresponding to the maximum current densities of about 0.1 A cm^{-1} . The two signs of the velocity correspond to the opposite drift directions; the plus sign is taken when the dc current flows towards the boundary. The parameters of the channel and the dielectric were $n_0 = 10^{11} \text{ cm}^{-2}$, $\epsilon_d = 12.8$ and $m = 0.067m_0$.

For numerical calculations, the continuous spectrum was approximated by several thousand modes, see (26), with the highest wavenumber equal to $100\kappa^{(0)}$. The accuracy was tested numerically and visually, by comparing E_x components of the incident and the reflected fields. They typically coincided for the distances up to 500 nm away from the channel, by which point the fields decreased about 20 000 times. The sum $\sum_i |E_{xi}^{(+)} + E_{xi}^{(-)}|^2$ calculated at 100 points within this range did not exceed 10^{-4} for moderate dc currents.

The important value is the reflection coefficient corresponding to the plasmons shown by points 1 and 2 in figure 2. As both analytical and numerical calculations show, the reflection coefficient is affected by the dc current, exceeding unity for positive currents, see figure 3. The dependence on the current is stronger for 1 THz than for

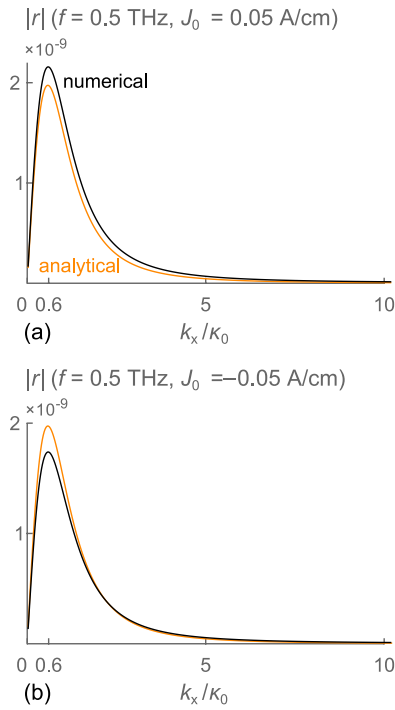


Figure 4. The analytical and numerical reflection coefficients agree for the continuous spectrum, both for positive (a) and negative (b) current directions. The reflection coefficients for the radiation modes (close to the origin) are small.

0.5 THz, because the plasmons are affected more by the current at higher frequencies, see figure 2.

The discrepancy between the analytical and numerical results is larger for the higher frequency and for the positive currents. It is probably due to the approximate solution of the plasmon dispersion relation (10). The perturbation solution (19) assumed linear variation of the wavenumbers with the drift velocity and ignored two of the four plasmons. This approximation becomes increasingly weaker, however, as the frequency increases and approaches point 5 in the dispersion diagram figure 2. Most affected will be plasmon 2 whose wavenumber will not only depend on the drift velocity in a complicated manner but also become comparable to that of plasmon 4. Because plasmon 2 is the reflected one for positive currents, the poor analytical approximation of its wavenumber may explain the higher discrepancy between the analytical and numerical results for the positive currents in figure 3.

According to (22), the increase in the reflection coefficient at one value of the dc current is the same as its decrease at the opposite value. The numerical calculations confirm that $|R_{J_0>0} R_{J_0<0}| \approx 1$.

As discussed above, a plasmon incident on the boundary at a negative dc current (point 2 in figure 2) can scatter also into two high-wavenumber plasmons (points 3 and 4 in figure 2). The corresponding reflection coefficients are, however, small. At 0.5 THz, for example, their absolute values are below 0.025 even for the highest dc current.

The analytical and numerical calculations agree well also for the reflection coefficients of the continuous-spectrum modes, as seen from figure 4 showing the reflection coefficients at 0.5 THz for opposite dc currents. Both the form of the

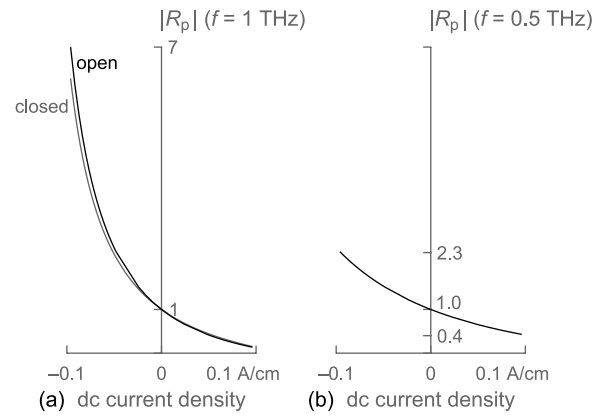


Figure 5. The plasmon power reflection coefficients reveal amplification for negative and de-amplification for positive currents. The effect is stronger at 1 THz (a) than at 0.5 THz (b). Although the channel is open, the plasmonic reflection coefficient (black line) is almost the same as in a closed channel (grey line).

curves and the position of the maxima agree, although there is a discrepancy in the maximum values. The reflection coefficients are the largest for $k_x \approx 0.6\kappa^{(0)} = 0.6\omega^2/\Omega_p^2$. In the radiative part of the spectrum, $k_x < \sqrt{\epsilon_d}k_0$, the reflection coefficients are small.

Further understanding of the plasmon reflection can be gained by looking at the power reflection coefficients. These were calculated from the amplitude ones and using the expression for the mode power (15). The power reflection coefficient depends on the dc current, see figure 5: its absolute value is larger than unity for negative dc currents and smaller than unity for positive ones. This behaviour is the inverse of that of the amplitude reflection coefficient, see figure 3. The power reflection coefficient, however, is the true indicator of the process nature. Hence, the plasmon is amplified on reflection when the dc current flows away from the boundary. It is de-amplified when the dc current flows towards the boundary. A closer examination of the electromagnetic and kinetic plasmon powers suggests the following explanation of the effect [26]. The electromagnetic power flows in the direction of plasmon propagation, towards the boundary for the incident and away from the boundary for the reflected plasmon. On the other hand, the direction of the kinetic power flow is determined by the direction of the electron drift both for the incident and the reflected plasmons. As a result, the total power is higher when the plasmon propagates along the drift, so that amplification occurs when the current flows away from the boundary. The amplification is signalled by the power reflection coefficient exceeding unity.

The situation is identical to the plasmon reflection in closed channels, discussed in detail in [26]. As a further demonstration of this similarity, figure 5(a) shows the reflection coefficient in a closed channel at 1 THz (grey line), where two conducting boundaries were placed at a distance of 200 nm above and below the channel, and the other parameters were the same as for the open channel. The two reflection coefficients have similar values. As could be expected, the plasmon amplification and de-amplification are stronger at 1 THz, figure 5(a), than at 0.5 THz, figure 5(b).

The power carried by all radiation modes turns out to be negligible. It can be estimated from (17) and the analytical expression for the reflection coefficient (23). For the radiation modes, $|\Gamma| \ll 1$ and $k_x \ll \kappa^{(0)}$ leading to

$$P_{\text{radiation}} \sim \frac{v_0^2}{\omega^2} \int_0^{\sqrt{\varepsilon_d} k_0} \frac{k_x^2}{\sqrt{\varepsilon_d k_0^2 - k_x^2}} dk_x \sim \frac{v_0^2}{c^2}, \quad (27)$$

a very small value.

The difference between open and closed 2D channels supporting dc currents lies, as it does for passive waveguides [27, 28, 33], in different approaches to solve the reflection problems due to different eigenmode spectra. In closed channels, the eigenmode spectrum consists of an infinite number of discrete modes: plasmons and waveguide modes. Each mode carries a finite amount of power, and all modes are mutually orthogonal. The reflection coefficients can be found as solutions of a matrix equation. By contrast, the eigenmode spectrum in open channels has both a discrete and a continuous parts. The discrete modes are the plasmons, carrying finite power. The continuous spectrum includes the radiative modes, carrying infinite power, see (17), and the evanescent modes. The resulting equations for the reflection coefficients, (24) and (25), are integral equations, which can be transformed into matrix ones by discretizing the integrals.

4. Conclusions

As the paper has shown, plasmons can be amplified upon reflection in open two-dimensional channels that carry dc currents. The analysis distinguishes itself by a rigorous treatment of the boundary conditions and by considering the complete spectrum of the eigenmodes. The amplification occurs when the dc current flows away from a conducting boundary; the opposite current direction leads to de-amplification.

Both processes will occur equally in a homogeneous channel confined between two conducting boundaries, and although this (and similar) symmetric configuration forms a plasmonic resonator, its roundtrip gain does not exceed unity. In this respect, open resonators could be expected to behave identically to the closed ones considered earlier [25, 26]. The qualitative and quantitative similarity between the reflection in open and closed channels, revealed here, suggests the same solutions for the open plasmonic oscillators as developed in the previous studies, for example, using channels with different dc electron densities.

Despite being open, the channels radiate a negligible amount of power during plasmon reflection. It confirms the need for additional coupling devices in practical plasmonic THz oscillators, such as grating couplers used in some experiments [35].

The analysis presented here augments the modal techniques developed earlier for closed resonators [25, 26]. Together, they provide a theoretical model that avoids *ad hoc* boundary conditions, which have dominated the recent research on plasmonic oscillators. Instead, they shift the emphasis to the device structure, in particular, structural asymmetry for achieving THz oscillations [25, 26].

Acknowledgments

The author is grateful to Professors R R A Syms and L Solymar for many helpful discussions.

References

- [1] Pines D and Schrieffer J R 1961 Collective behavior in solid-state plasmas *Phys. Rev.* **124** 1387–400
- [2] Hutson A R, McFee J H and White D L 1961 Ultrasonic amplification in CdS *Phys. Rev. Lett.* **7** 237–9
- [3] Gunn J B 1963 Travelling-wave interaction between the optical modes of a polar lattice and a stream of charge carriers *Phys. Lett.* **4** 194–5
- [4] Solymar L and Ash E A 1966 Some travelling-wave interactions in semiconductor theory and design considerations *Int. J. Electr.* **20** 127–48
- [5] Krashennnikov M V and Chaplik A V 1980 Instabilities of two-dimensional plasma waves *Sov. Phys.—JETP* **52** 279–82
- [6] Allen Jr. S J, Derosa F, Bhat R, Dolan G and Tu C W 1985 Standing charge density waves driven by electron drift in patterned (Al, Ga)As/GaAs heterostructures *Physica B+C* **134** 332–6
- [7] Hawrylak P and Quinn J J 1986 Amplification of bulk and surface plasmons in semiconductor superlattices *Appl. Phys. Lett.* **49** 280–2
- [8] Gómez Rivas J, Kuttge M, Haring Bolivar P, Kurz H and Sánchez-Gil J A 2004 Propagation of surface plasmon polaritons on semiconductor gratings *Phys. Rev. Lett.* **93** 256804
- [9] Veksler D, Teppe F, Dmitriev A P, Kachorovskii V Yu, Knap W and Shur M S 2006 Detection of terahertz radiation in gated two-dimensional structures governed by dc current *Phys. Rev. B* **73** 125328
- [10] Hendry E, Garcia-Vidal F J, Martin-Moreno L, Gómez Rivas J, Bonn M, Hibbins A P and Lockyear M J 2008 Optical control over surface-plasmon-polariton-assisted thz transmission through a slit aperture *Phys. Rev. Lett.* **100** 123901
- [11] Mikhailov S A 1998 Plasma instability and amplification of electromagnetic waves in low-dimensional electron systems *Phys. Rev. B* **58** 1517–32
- [12] Sydoruk O, Shamonina E and Solymar L 2010 Solid-state traveling-wave amplifiers and oscillators in the thz range effect of electron collisions *Eur. Phys. J. D* **59** 233–40
- [13] Riyopoulos S 2005 Thz instability by streaming carriers in high mobility solid-state plasmas *Phys. Plasmas* **12** 070704
- [14] Kukhtaruk S M 2008 High-frequency properties of systems with drifting electrons and polar optical phonons *Sem. Phys. Quant. Electr. Optoelectr.* **11** 43–9
- [15] Sydoruk O, Kalinin V and Solymar L 2010 Terahertz instability of optical phonons interacting with plasmons in two-dimensional electron channels *Appl. Phys. Lett.* **97** 062107
- [16] Sydoruk O, Shamonina E, Kalinin V and Solymar L 2010 Terahertz instability of surface optical-phonon polaritons that interact with surface plasmon polaritons in the presence of electron drift *Phys. Plasmas* **17** 102103
- [17] Dyakonov M and Shur M 1993 Shallow water analogy for a ballistic field-effect transistor new mechanism of plasma wave generation by a dc current *Phys. Rev. Lett.* **71** 2465–8
- [18] Crowne F J 1997 Contact boundary conditions and the dyakonov–Shur instability in high electron mobility transistors *J. Appl. Phys.* **82** 1242–54
- [19] Cheremisin M V and Samsonidze G G 1999 D'yakonov–Shur instability in a ballistic field-effect transistor with a spatially nonuniform channel *Semiconductors* **33** 578–85

- [20] Crowne F J 2000 Dyakonov–Shur plasma excitations in the channel of a real high-electron mobility transistor *J. Appl. Phys.* **87** 8056–63
- [21] Dyakonov M and Shur M S 2005 Current instability and plasma waves generation in ungated two-dimensional electron layers *Appl. Phys. Lett.* **87** 111501
- [22] Sydoruk O, Syms R R A and Solymar L 2010 Plasma oscillations and terahertz instability in field-effect transistors with Corbino geometry *Appl. Phys. Lett.* **97** 263504
- [23] Pierce J R 1944 Limiting stable current in electron beams in the presence of ions *J. Appl. Phys.* **15** 721–6
- [24] Sze S M and Kwok K. Ng 2007 *Physics of Semiconductor Devices* (Hoboken, NJ: Wiley)
- [25] Sydoruk O, Syms R R A and Solymar L 2012 Distributed gain in plasmonic reflectors and its use for terahertz generation *Opt. Express* **20** 19618–27
- [26] Sydoruk O, Syms R R A and Solymar L 2012 Amplifying mirrors for terahertz plasmons *J. Appl. Phys.* **112** 104512
- [27] Shevchenko V V 1971 *Continuous Transitions in Open Waveguides* (Boulder, CO: Golem Press)
- [28] Marcuse D 1982 *Light Transmission Optics* (New York: Van Nostrand Reinhold)
- [29] Vural B and Bloom S 1966 Streaming instabilities in solids and the role of collisions *IEEE Trans. Electron. Dev.* **13** 57–63
- [30] Ó Súilleabháin L C, Hughes H P, Churchill A C, Ritchie D A, Grimshaw M P and Jones G A C 1994 Raman studies of plasmon modes in a drifting two-dimensional electron gas *J. Appl. Phys.* **76** 1701–5
- [31] Fetter A L 1973 Electrodynamics of layered electron gas. I. Single layer *Ann. Phys.* **81** 367–93
- [32] Rigrod W W 1960 Power flow and stored energy in thin electron beams *J. Appl. Phys.* **31** 1147–53
- [33] Collin R E 2001 *Foundations for Microwave Engineering* (Hoboken, NJ: Wiley-IEEE Press)
- [34] Bresler A D, Joshi G H and Marcuvitz N 1958 Orthogonality properties for modes in passive and active uniform wave guides *J. Appl. Phys.* **29** 794–9
- [35] Otsuji T, Meziani Y M, Nishimura T, Suemitsu T, Knap W, Sano E, Asano T and Popov V V 2008 Emission of terahertz radiation from dual grating gate plasmon-resonant emitters fabricated with InGaP/InGaAs/GaAs material systems *J. Phys. Condens. Matter* **20** 384206